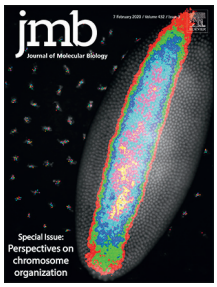

Small Molecular Inhibitors Block TRPM4 Currents in Prostate Cancer Cells, with Limited Impact on Cancer Hallmark Functions

Anna Borgström [1]*, Barbara Hauert [1], Sven Kappel [1], Eugenio Zoni [2], Mirjam Kiener [2], Paulina Stokłosa [1], Roland Baur [1], Martin Spahn [3], Marianna Kruithof-de Julio [2] and Christine Peinelt [1]*

*1 - **Institute of Biochemistry and Molecular Medicine,** National Center of Competence in Research NCCR TransCure, University of Bern, Bern, Switzerland*

*2 - **Urology Research Laboratory,** Department of Urology and Department for Biomedical Research, University of Bern, Bern, Switzerland*

*3 - **Urology Center Boxler and Spahn,** Bern, Lindenhofspital Bern, Switzerland; Department of Urology, University of Duisburg-Essen, Essen, Germany*

***Correspondence to Anna Borgström and Christine Peinelt:** anna.borgstroem@ibmm.unibe.ch (A. Borgström), christine.peinelt@ibmm.unibe.ch (C. Peinelt)*

https://doi.org/10.1016/j.jmb.2020.09.024

Edited by Vera Moiseenkova-Bell

Abstract

Transient receptor potential melastatin 4 (TRPM4) is a broadly expressed Ca^{2+} activated monovalent cation channel that contributes to the pathophysiology of several diseases.

For this study, we generated stable CRISPR/Cas9 TRPM4 knockout (K.O.) cells from the human prostate cancer cell line DU145 and analyzed the cells for changes in cancer hallmark functions. Both TRPM4-K.O. clones demonstrated lower proliferation and viability compared to the parental cells. Migration was also impaired in the TRPM4-K.O. cells. Additionally, analysis of 210 prostate cancer patient tissues demonstrates a positive association between TRPM4 protein expression and local/metastatic progression. Moreover, a decreased adhesion rate was detected in the two K.O. clones compared to DU145 cells.

Next, we tested three novel TRPM4 inhibitors with whole-cell patch clamp technique for their potential to block TRPM4 currents. CBA, NBA and LBA partially inhibited TRPM4 currents in DU145 cells. However, none of these inhibitors demonstrated any TRPM4-specific effect in the cellular assays.

To evaluate if the observed effect of TRPM4 K.O. on migration, viability, and cell cycle is linked to TRPM4 ion conductivity, we transfected TRPM4-K.O. cells with either TRPM4 wild-type or a dominant-negative mutant, non-permeable to Na^+. Our data showed a partial rescue of the viability of cells expressing functional TRPM4, while the pore mutant was not able to rescue this phenotype. For cell cycle distribution, TRPM4 ion conductivity was not essential since TRPM4 wild-type and the pore mutant rescued the phenotype.

In conclusion, TRPM4 contributes to viability, migration, cell cycle shift, and adhesion; however, blocking TRPM4 ion conductivity is insufficient to prevent its role in cancer hallmark functions in prostate cancer cells.

© 2020 The Author(s). Published by Elsevier Ltd. This is an open access article under the CC BY license (http://creativecommons.org/licenses/by/4.0/).

source: https://doi.org/10.7892/boris.149006 | downloaded: 4.1.2021

0022-2836/© 2020 The Author(s). Published by Elsevier Ltd.This is an open access article under the CC BY license (http://creativecommons.org/licenses/by/4.0/).

Please cite tts article as: A. Borgström, B. Hauert, S. Kappel, et al., Small Molecular Inhibitors Block TRPM4 Currents in Prostate Cancer Cells, with Limited Impact on Cancer Hallmark Functions, *Journal of Molecular Biology*, https://doi.org/10.1016/j.jmb.2020.09.024

Background

Each year around 1.3 million men worldwide are diagnosed with prostate cancer.[1] After lung cancer, prostate cancer is the most frequently diagnosed malignancy in men, and it is the fifth leading cause of cancer-related death in men.[1] Androgen deprivation therapy (ADT) is commonly used as initial treatment of prostate cancer. This therapy can be initially efficient, however, most cases develop resistance to ADT and transform into castration-resistant prostate cancer (CRPC). In that case, chemotherapy is the preferred continued treatment, but CRPC also tends to develop resistance to the chemotherapeutic drugs and transform into dual-resistant prostate cancer. Therefore, with the frequent transformation of prostate cancer into CRPC, the need for new therapies is growing.[2,3]

In a recent study, Berg and colleagues demonstrated a positive correlation between transient receptor potential melastatin 4 (TRPM4) channel protein overexpression in combination with a high histoscore (H-score) and increased risk of recurrence after radical prostatectomy.[4] Moreover, another study aimed at identifying cancer-driver genes for prostate cancer described TRPM4 as a cancer-driver gene in androgen-independent prostate cancer cells.[5]

TRPM4 is a Ca^{2+} activated monovalent cation channel, which belongs to the family of transient receptor potential (TRP) channels. TRPM4 is widely expressed in various organs, although its expression is the highest in prostate and colon.[6] TRPM4 conducts monovalent cations, such as Na^+ and K^+, without significant permeability toward Ca^{2+}.[7] TRPM4 is involved in intracellular Ca^{2+} signaling, as Na^+ influx, after activation of TRPM4, may depolarize the plasma membrane and thereby decrease the driving force for Ca^{2+} influx via store-operated Ca^{2+} entry (SOCE).[8–13]

Several studies comparing the expression levels of TRPM4 in malignant prostate tissue and healthy prostate glands reported that TRPM4 mRNA was significantly elevated in tumor samples (reviewed in [14]). Particularly, TRPM4 mRNA expression levels were increased in premalignant human prostatic intraepithelial neoplasia (PIN).[15] TRPM4 was shown to contribute to the proliferation of prostate and cervical cancer cells, through the activity of GSK3β and β-catenin[16,17] and was reported to contribute to the migration and invasion of prostate cancer cells.[9,17,18] Additionally, a mass spectrometry-based proteomics study found TRPM4 to be associated with focal adhesion (FA)-related proteins. In addition to its focal adhesion localization, TRPM4 was reported to regulate FA turnover.[19,20] Recently, TRPM4 was identified to be negatively regulated by microRNA-150 (miR150). Upregulation of miR150 resulted in inactivation of β-catenin signaling and suppression of epithelial mesenchymal transition (EMT) as well as cell cycle shift in PC3 prostate cancer cells.[21]

Due to its overexpression and involvement in cancer hallmark functions of prostate cancer, TRPM4 is an interesting drug target candidate. However, due to the lack of selective and potent inhibitors, TRPM4 has not yet been validated as such. The two most commonly used inhibitors for studies of TRPM4 to date are flufenamic acid and 9-phenanthrol. However, both have been reported to have low potency[22,23] and a long list of off-targets.[24] Therefore, new selective inhibitors are required to accurately and efficiently study the role of TRPM4 and its ion conductivity in different disease model systems. Recently, a new potent and selective inhibitor of TRPM4, so-called compound 5 (4-chloro-2-(2-chlorophenoxy) acetamido)benzoic acid, now named CBA), was discovered.[25,26] CBA blocks TRPM4 current both in cells overexpressing TRPM4 and in the LNCaP prostate cancer cell line, expressing endogenous TRPM4.[26] Moreover, CBA showed good selectivity over other TRP channel family members (TRPV1, TRPV3, TRPV6, TRPM5, TRPM7, TRPM8).[26]

Here we investigate whether CBA or any of its new derivative compounds are useful tools to study the role of TRPM4 in prostate cancer and could contribute to the development of new clinical drug candidates. In this study, we show impaired cell viability, migration, and changes in cell adhesion in TRPM4 CRISPR/Cas9 knockout (K.O.) cells. We investigated the underlying mechanism with rescue cells expressing TRPM4 or a dominant negative construct, which is unable to conduct Na^+ (TRPM4-D984A).

Results

Decreased migration, proliferation, and changes in cell cycle distribution in TRPM4 knockout cells

To study the impact of TRPM4 on viability and migration in prostate cancer cells, we generated stable TRPM4-K.O. cells from the DU145 prostate cancer cell line using CRISPR/Cas9 technique. In TRPM4-K.O. clones 1 and 2, TRPM4 protein and mRNA expression were absent (Supplementary Figure S1a and b). TRPM4-specific currents have been identified in DU145 in the past,[9] but due to technical limitations of the TRPM4 siRNA downregulation, the proportion of TRPM4 in Ca^{2+} activated non-selective current (I_{CAN}) remained unclear. TRPM4 currents were evoked with 10 μM Ca^{2+} in the patch pipette in whole-cell patch clamp configuration. Currents were extracted at −80 mV and +80 mV (normalized to cell capacitance) and plotted as current density (CD) versus time (Figure 1a). Under these conditions, a current of ~40 pA/pF developed in

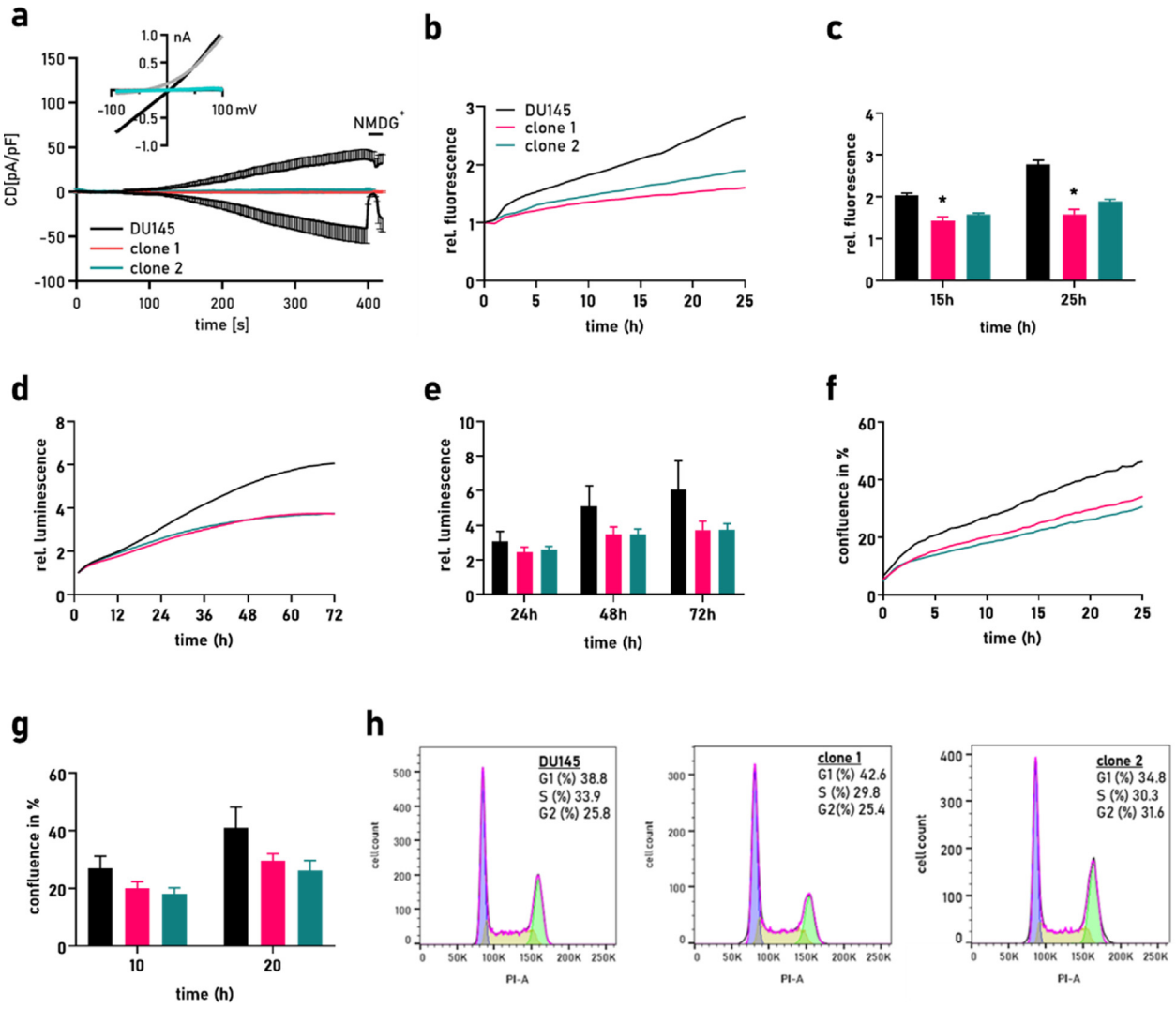

Figure 1. TRPM4 knockout affects important cellular functions in DU145. (a) Whole-cell patch clamp data from DU145 and two K.O. clones (clones 1 and 2). Currents were evoked with 10 μM Ca^{2+} in the patch pipette and normalized to cell size. $NMDG^+$ was applied on cells at $t = 400$ s. Current density (CD), displayed as mean +/− SEM, is plotted versus time. Inset: extracted current-voltage relationship curves (IVs) at $t = 394$ s in black and during $NMDG^+$ application at $t = 408$ s in gray ($n = 6$ for DU145, $n = 6$ for clone 1, $n = 5$ for clone 2). (b) Transwell migration assay of DU145 and TRPM4-K.O. clones 1 and 2: relative fluorescence was recorded over 25 h and plotted versus time. (c) Bar graph of data in (b) at 15 and 25 h displayed as mean + SEM, duplicates, $n = 3$. (d) Cell viability of DU145 and clones 1 and 2 evaluated with RealTime-Glo MT assay, plotted over time as relative luminescence, normalized to the value at $t = 0$. (e) Bar graph of data from (d) at 24, 48, and 72 h, displayed as mean + SEM, triplicates, $n = 3$. (f) Cell confluence was evaluated with the IncuCyte imaging system. Images were acquired every 30 min over 24 h and confluence in % was plotted versus time. (g) Bar graph of cell confluence data from (f) plotted as mean + SEM, $n = 3$. (h) Representative propodium iodide (PI)-staining histograms. Cell cycle distribution displayed in % of cells, as mean of seven independent experiments. For all assays above, a value of $p < 0.05$ was considered statistically significant.

DU145. The current–voltage relationship curve (IV) at $t = 394$ s, displaying a positive reversal potential characteristic of TRPM4, can be seen as an inset in Figure 1a. Upon replacement of Na^+ in the bath solution with the impermeable cation $NMDG^+$ (at $t = 400$ s), the inward current was inhibited, demonstrating that the recorded currents were carried by monovalent Na^+ ions. Current development was absent in TRPM4-K.O. clones 1 and 2, indicating that in DU145 I_{CAN} is carried exclusively by TRPM4 (Figure 1a).

Impairment of TRPM4 decreased migration in other prostate cancer cell systems.[9,17,21] To investigate migration in our DU145 K.O. system, we set up a fluorescence-based transwell migration assay with FCS as chemoattractant (Figure 1b). As

displayed in Figure 1c, migration was decreased in clones 1 and 2 (23–43%) compared to the parental cell line at the indicated time points. The effect of TRPM4 K.O. on migration was confirmed with a label-free migration assay on the xCELLigence® RTCA DP system. Here, the migration was strongly decreased by 36–66% after 10 h, with a 49–79% slower slope at 5–10 h in both K.O. clones (significant for clone 2) compared to DU145 (Supplementary Figure S2a–c).

Next, the effect of TRPM4 knockout on cell viability and proliferation was evaluated (Figure 1d–g). Cell viability was determined with a real-time kinetic assay over 72 h. TRPM4-K.O. clones 1 and 2 displayed lower viability compared to DU145 cells (Figure 1d). After 72 h, the two K.O. clones demonstrated 38% lower viability compared to the parental cells (Figure 1e). Proliferation was evaluated in real time with the IncuCyte S3 system and was read out as increased cell confluence against time (Figure 1f). Proliferation was reduced in both TRPM4-K.O. clones compared to DU145 after 10 and 20 h with 30–37% reduction at 20 h (Figure 1g).

Cell cycle distribution plays an important role in the regulation of proliferation, and TRPM4 has been shown to affect cell cycle distribution in the past.[21,27,16] Therefore, cell cycle distribution of DU145 and TRPM4-K.O. clones was determined with PI staining and flow cytometry. Clone 1 displayed a tendency for more cells in G1-phase compared to DU145 (Figure 1h). This is in line with previously published data from another prostate cancer cell line,[21] and data from cervical[16] and colorectal cancer cells.[27] However, in clone 2 an increase in G2-phase and a slight decrease in G1-phase were detected.

Altogether, as previously published for other cellular prostate cancer systems, DU145 TRPM4 CRISPR/Cas9 K.O. clones show a reduction in cancer hallmark functions cell viability, proliferation, migration and a slight shift in cell cycle.

TRPM4 knockout results in impaired cell adhesion

Corresponding to the above experiments, proliferation was decreased by 34–41% at 48 h compared to the parental cells in the label-free proliferation assay from xCELLigence (Figure 2a and Supplementary Figure S2d and e). In addition to the above findings on proliferation, the impedance-based xCELLigence assay revealed a discrepancy between the parental cells and the two K.O. clones in the first 3–5 h (Figure 2b). It should be noted that a proliferation cycle takes ~34 h for DU145 cells.[28] Hence, the early difference (up to 5 h) is not the result of decreased proliferation, but rather is connected to differences in adhesion and cell spreading.[29] Here we quantified the differences in cell adhesion by calculating the slope at 2–5 h. The two TRPM4-K.O. cell lines displayed up to 78% decreased adhesion rate when compared to DU145 (Figure 2c).

To further investigate changes in cell adhesion by TRPM4 knockout, we performed an image-based assay. The IncuCyte assay allows visualization and analysis of the adhesion process. Cell adhesion of DU145 and TRPM4-K.O. clones was quantified as cell confluence at different time points (Figure 2d and e). Cells adhering to the surface are more spread and flatter than the non-adherent spherical cells. Therefore, non-adherent cells will add less to the total cell confluence. Moreover, these cells will appear smaller. Clones 1 and 2 showed cell confluence of 15–16% at 6 h compared to DU145 cells, which averaged 22% confluence (Figure 2d and e). The average size of objects (cells) was analyzed with the IncuCyte software. Quantification of the average object size showed a smaller size of clones 1 and 2 compared to DU145 (Figure 2f), indicating that these cells are less adherent or less spread on the well surface than the parental cells. Figure 2g shows representative images of DU145 cells (upper panel), TRPM4-K.O. clone 1 (middle panel), and TRPM4-K.O. clone 2 (lower panel) at 1.5 or 5 h at 10x magnification (two left panels). Enlargements of the same images are displayed in the two right-hand panels. After 5 h, the two TRPM4-K.O. clones were more spherical and less adherent than the parental cells. Additionally, the images indicate that most cells from the parental cell line were adherent at 5 h.

Overall, our data suggest decreased adhesion and cell spreading in the two TRPM4-K.O. clones compared to DU145 cells.

Novel TRPM4 inhibitors block endogenous TRPM4 currents

Recently, three small molecular inhibitors of TRPM4, CBA ((4-chloro-2-(2-chlorophenoxy) acetamido)benzoic acid), NBA (4-chloro-2-(1-naphthyloxyacetamido)benzoic acid), and LBA (4-chloro-2-(2-(4-chloro-2-methylphenoxy)propanamido) benzoic acid)), have been described.[25,26] CBA was previously positively evaluated as a potent inhibitor of endogenous TRPM4 currents in LNCaP prostate cancer cell line.[26] For the purpose of comparing our data and IC_{50}-values with previous published data of CBA treated LNCaP cells (IC_{50} for CBA 1.1 ± 0.3 μM), we here assess the ability of CBA, NBA, and LBA to block endogenous TRPM4 currents in LNCaP cells. TRPM4-specific currents were evoked with 10 μM Ca^{2+} in the pipette solution in whole-cell patch clamp configuration. After current development (at t = 280 s), 3 μM of NBA, LBA, or CBA was applied for 120 s (Figure 3a–c). After 400 s, standard bath solution was applied to wash out the inhibitors. The TRPM4 current–voltage relationship (IV) before (t = 276 s)

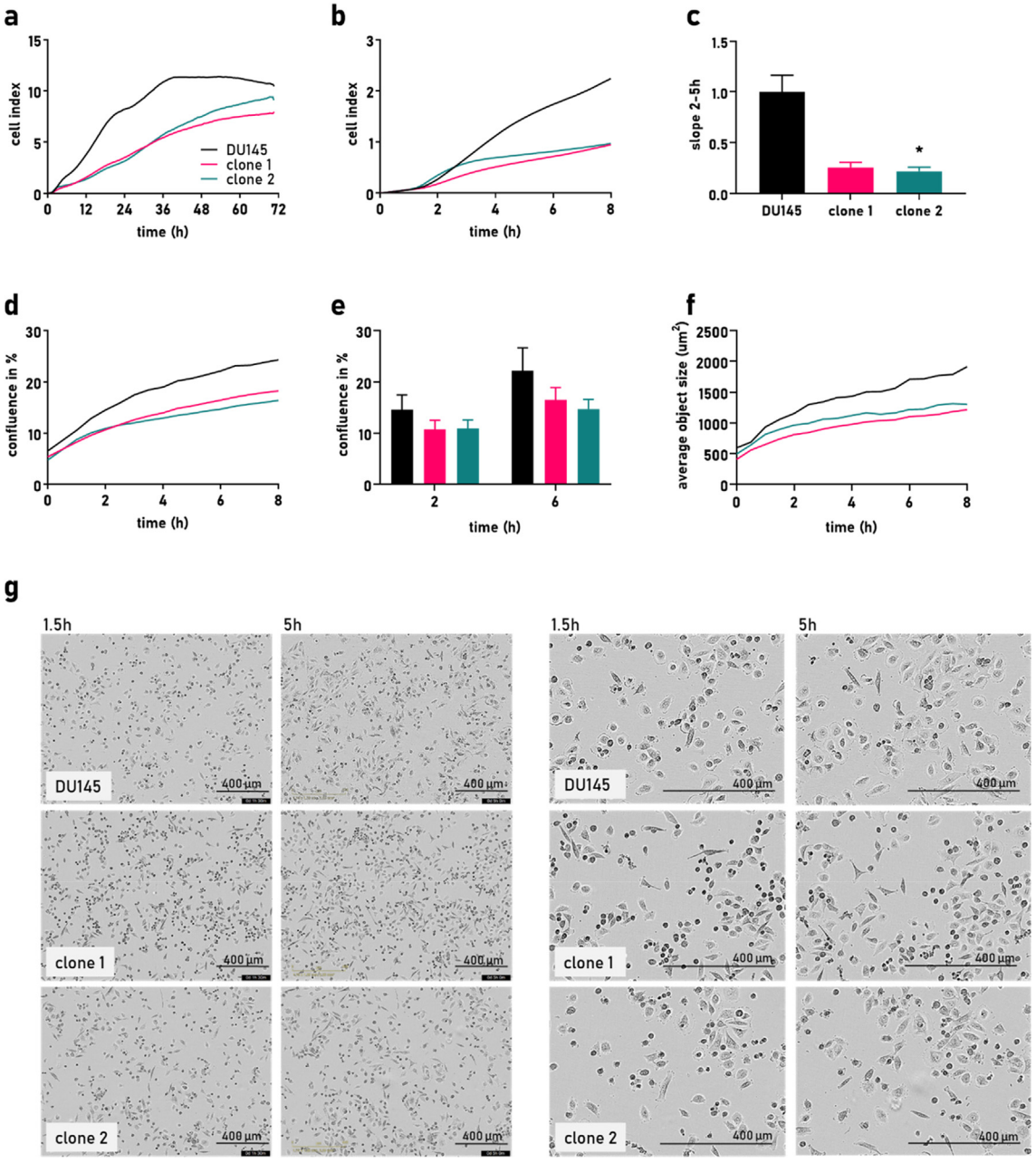

Figure 2. Alterations of cell adhesion in TRPM4 knockout cells. (a) Cell proliferation was evaluated with impedance-based xCELLigence system. Growth rates were plotted as cell index over 72 h. (b) First 8 h from graph (a) displayed. (c) Bar graph of the slope at 2–5 h from (b). Data is presented as mean + SEM from four independent experiments. (d) Cell confluence was analyzed with live-cell imaging system and plotted in % versus time. (e) Comparison of cell confluence of DU145 and clones 1 and 2 at 2 and 6 h after seeding (1×10^5 cells per well). Each experiment was repeated at least three times and is displayed as mean + SEM. (f) Average size of objects (cells) analyzed based on the data collected in (d), and plotted as average size in μm^2 over time 10 h as mean of three experiment. (g) Representative images from (d) at 1.5 and 5 h post seeding. Right panel shows magnification of the images from the left panel. Scale bar = 400 µm. *p*-value < 0.05 was considered significant.

and during (t = 396 s) application of the inhibitor is shown as an inset in the current density graphs (Figure 3a–c). Each compound (LBA, NBA, and CBA) inhibited TRPM4 currents at a dose of 3 µM (Figure 3a–c). The calculated IC_{50} values from the dose response curves were 0.74 ± 2.0 µM for LBA and 0.16 ± 2.4 µM for NBA (Figure 3d and e). Upon application of bath solution, the current block by LBA and NBA was not reversible, while the block by CBA was partly reversible (56% recovered; Figure 3f). All IC_{50} values are in good agreement with the IC_{50} values previously assessed with

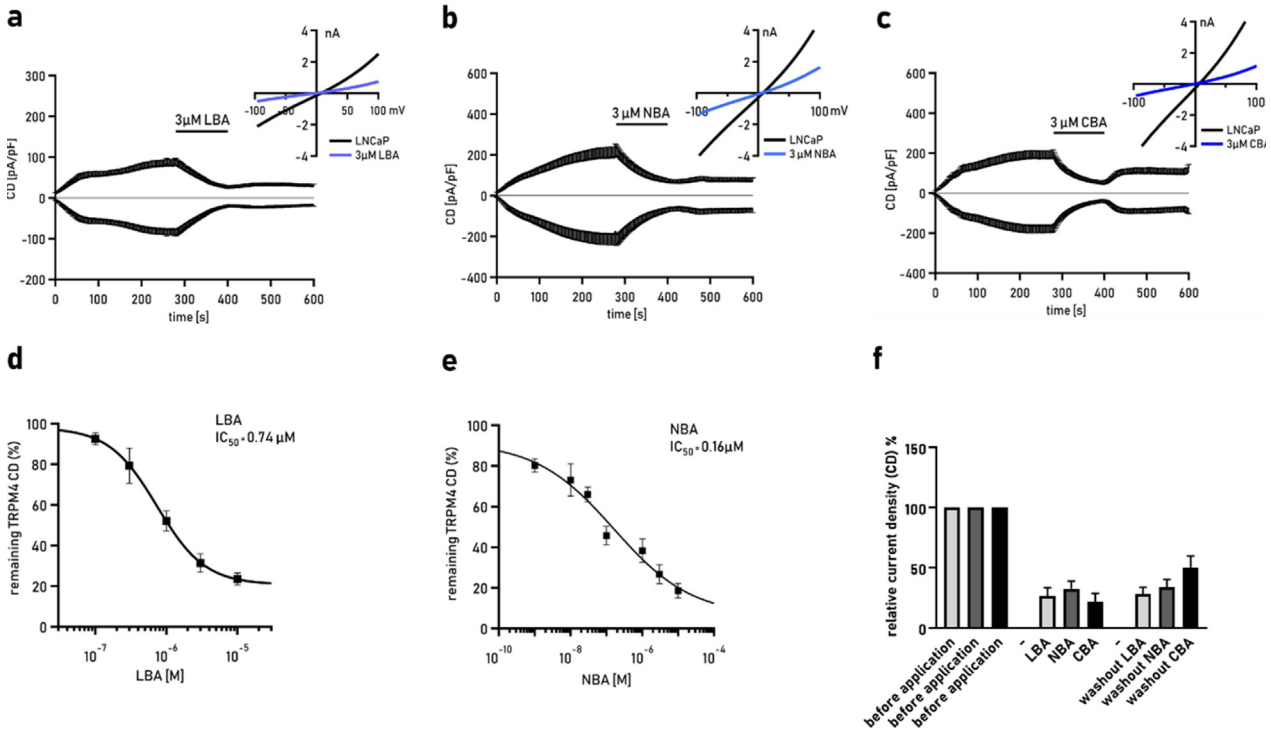

Figure 3. Novel TRPM4 inhibitors block endogenous TRPM4 in LNCaP cells. (a) Whole-cell patch clamp data from LNCaP. Currents were evoked with 10 μM Ca^{2+} in the patch pipette and normalized to cell size. Current density (CD), displayed as mean +/− SEM, is plotted versus time and 3 μM LBA was applied from 280–400 s. Inset: IV curves at $t = 196$ s and $t = 396$ s ($n = 12$). (b) Same as (a) for NBA ($n = 15$). (c) Same as (a) for CBA ($n = 6$). (d) Average TRPM4 CD +/− SEM was plotted against LBA concentrations ($n = 6$ for 0.1 μM, $n = 5$ for 0.3 μM, $n = 7$ for 1 μM, $n = 12$ for 3 μM, $n = 5$ for 10 μM). Dose-response curve was fitted with a Hill equation and IC_{50} value was calculated to be 0.74 ± 2.0 μM. (e) Average TRPM4 CD +/− SEM plotted against NBA concentrations ($n = 8$ for 0.001 μM, $n = 5$ for 0.03 μM, $n = 7$ for 0.01 μM, $n = 6$ for 0.1 μM, $n = 7$ for 1 μM, $n = 15$ for 3 μM, $n = 6$ for 10 μM). Dose-response curve was fitted with a Hill equation and IC_{50} value was calculated to be 0.16 ± 2.4 μM. (f) Evaluation of current densities before application, during inhibitor treatment (3 μM), and after washout of the three inhibitors. Data normalized to the CD before inhibitor application and displayed as mean + SEM.

inside-out patch clamp recordings of excised membranes from HEK293 TRPM4 overexpressing cells and the IC_{50} of CBA in LNCaP.[26] Nevertheless, it is worth mentioning that even at high doses (10 μM), the remaining current was about 20–30% for all three inhibitors.

Altogether, the three compounds block endogenous TRPM4 currents in the LNCaP prostate cancer cell line. None of the inhibitors entirely blocked TRPM4 currents. While the block with CBA was partly reversible, inhibition by LBA und NBA was seemingly irreversible.

Evaluation of cellular functions with TRPM4 inhibitor treatment

Given the contribution of TRPM4 to cancer hallmark functions, we next investigated the effect of CBA on proliferation and migration. First, we verified the ability of CBA to block the Ca^{2+} induced TRPM4 current in DU145 cells. At concentrations of 3 and 50 μM, CBA blocked 55 ± 6% and 65 ± 7% of endogenous TRPM4 currents in the DU145 prostate cancer cell line (Figure 4a and b). Next, the effect of CBA on proliferation was evaluated in DU145 cells with the label-free xCELLigence proliferation assay. Cells were either untreated, treated with different concentrations of CBA, or with DMSO as a control. Figure 4c displays the cell index for each condition after 20 h. A slight decrease in proliferation was observed with the highest CBA concentrations tested (≥25 μM). However, DMSO control treatment also decreased proliferation, and low concentrations of CBA did not block, but seemingly induced a slight increase in proliferation. We next evaluated the effect of CBA on cell migration. Two different concentrations (10 μM and 50 μM) were applied in a transwell migration assay and a decrease in migration was detected for cells treated with 50 μM CBA (Figure 4d: over time; 4e: slope; and 4f: cell index). Overall, only high doses (≥25 μM) of CBA decreased proliferation and migration.

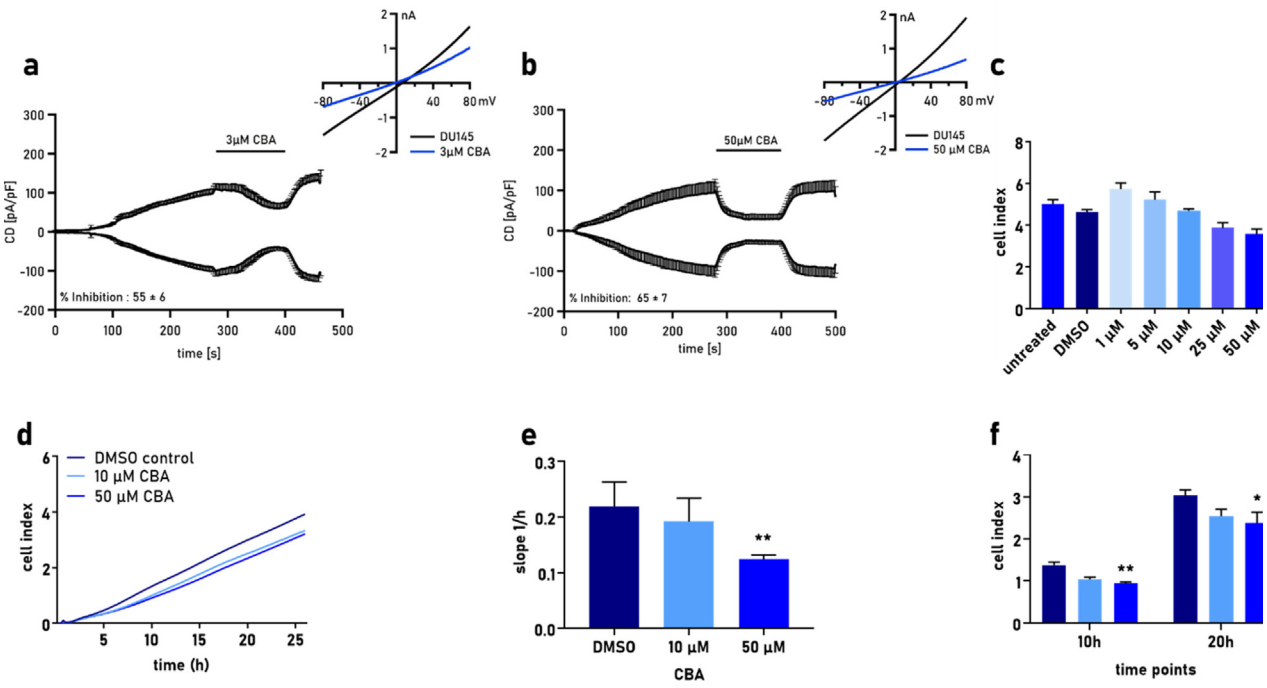

Figure 4. TRPM4 inhibitors evaluated for effects on migration and proliferation in DU145 cells. (a) Whole-cell patch clamp data from DU145. Currents were evoked with 10 μM Ca^{2+} in the patch pipette and normalized to cell size. CD, displayed as mean +/− SEM, is plotted versus time and 3 μM CBA was applied from 280–400 s (n = 6). Inset: corresponding IV curves, t = 276 s shown in black and t = 396 s during 3 μM CBA application in blue. (b) Same as (a) but with application of 50 μM CBA (n = 6). (c) Proliferation assay with CBA titration of 0–50 μM: cell index at 20 h is plotted as mean + SEM. (d) Migration assay of DU145 with CBA treatment plotted as cell index versus time. (e) Slope of cell index at 5–20 h from migration assay in (d) is plotted for control (DMSO), 10 μM, and 50 μM CBA. (f) Cell index from migration assay in (d) is plotted at 10 and 20 h of migration. Migration assay was repeated at least four times in triplicates. Values are displayed as mean + SEM.

We next tested the TRPM4 specificity of this effect. CBA was evaluated for its effect on proliferation and migration in the two TRPM4-K.O. clones. High doses (≥25 μM) of CBA decreased proliferation of TRPM4-K.O. clones (Figure 5a: clone 1; 5b: clone 2) similar to the parental TRPM4-expressing DU145. The CBA-induced decrease in proliferation, normalized to the DMSO control, for DU145 and the two K.O. clones is summarized in Figure 5c. No difference between the parental DU145 and the two TRPM4-K.O. clones was observed. Furthermore, the impact of CBA on migration of TRPM4-K.O. cells was evaluated. TRPM4-K.O. clones 1 and 2 were treated with 10 and 50 μM CBA in a transwell migration assay (Figure 5d). In both clones, 50 μM CBA decreased the migration to a similar extent as in the parental DU145 cells (Figure 5e). Finally, the effect of NBA and LBA in DU145 was analyzed with patch clamp experiments. At a concentration of 50 μM, NBA blocked 88 ± 9 % of the endogenous TRPM4 currents in DU145 (Figure 5f) and 50 μM of LBA blocked 85 ± 7 % of TRPM4 (Figure 5h). Next, the effect of NBA and LBA on proliferation was analyzed in DU145 and the two TRPM4-K.O. clones. Here, no significant impact on proliferation was observed at any of the time points (Figure 5g and i).

In conclusion, compounds CBA, NBA, and LBA partly blocked endogenous TRPM4 currents. However, their effect on proliferation and migration at very high doses is not specific to TRPM4.

TRPM4 ion conductivity is important for rescue of cell viability

Our results show that the three TRPM4 blockers failed to affect cellular functions. We hypothesized that TRPM4 ion conductivity is not essential for the effect on viability and migration observed with the TRPM4-K.O. cells. To address the role of ion conductivity in the observed viability and migration phenotypes, we generated stable TRPM4 re-expressing cells from the two TRPM4-K.O. cell lines. Clones 1 and 2 were stably transfected with either TRPM4 wild-type (TRPM4-wt) or a dominant negative mutant TRPM4 (TRPM4-D984A), which forms a non-conductive full-size protein.[27,30] TRPM4 expression levels in these cells were evaluated on protein and mRNA level (Supplementary Figure S3), and the functionality of TRPM4 was confirmed with whole-cell patch

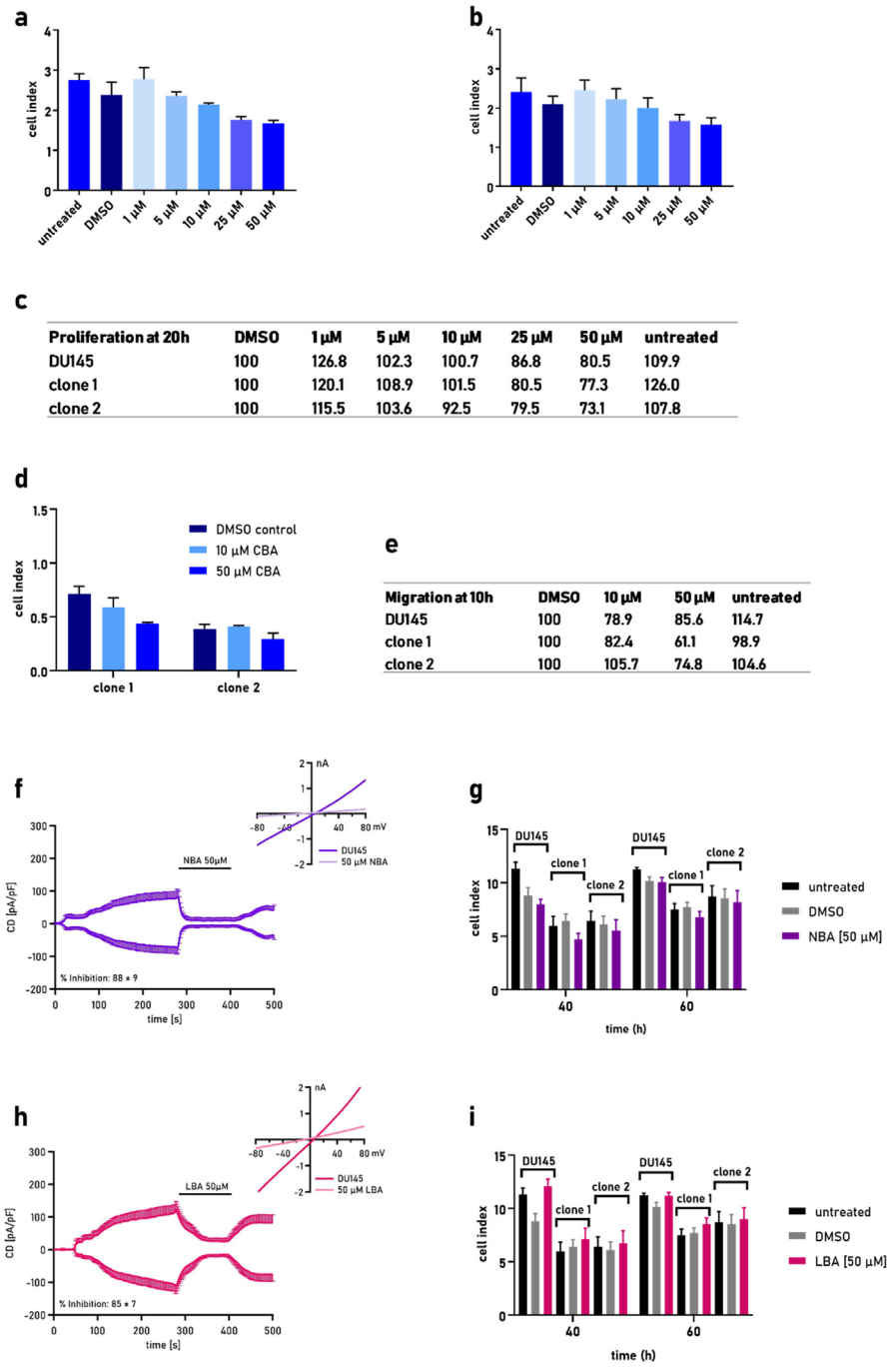

Proliferation at 20h	DMSO	1 µM	5 µM	10 µM	25 µM	50 µM	untreated
DU145	100	126.8	102.3	100.7	86.8	80.5	109.9
clone 1	100	120.1	108.9	101.5	80.5	77.3	126.0
clone 2	100	115.5	103.6	92.5	79.5	73.1	107.8

Migration at 10h	DMSO	10 µM	50 µM	untreated
DU145	100	78.9	85.6	114.7
clone 1	100	82.4	61.1	98.9
clone 2	100	105.7	74.8	104.6

Figure 5. TRPM4 blockers in TRPM4-knockout cell lines. (a) Proliferation assay of clone 1 treated with 0–50 µM CBA. Data is displayed as cell index at 20 h of treatment. (b) Same as (a) for clone 2. (c) Table of proliferation cell index at 20 h upon inhibitor treatment for parental DU145, clones 1 and 2. Values are normalized to the cell index of corresponding DMSO controls. (d) Transwell migration assay of clones 1 and 2 during CBA treatment of 10 and 50 µM at 10 h of migration. (e) Table of migration cell index at 10 h upon inhibitor treatment of DU145, clone 1 and clone 2. Values are normalized to the corresponding DMSO controls. (f) Whole-cell patch clamp data from DU145. Currents were evoked with 10 µM Ca^{2+} in the patch pipette and normalized to cell size. CD, displayed as mean +/− SEM, is plotted versus time and 50 µM NBA was applied from 280–400 s (n = 6). Inset: corresponding IV curves, t = 276 s shown in black and t = 396 s during 50 µM NBA application in purple. (g) Proliferation assay with 50 µM NBA treatment of DU145, clones 1 and 2. Cell index upon 40 or 60 h of inhibitor treatment is displayed. (h) Same as (f) for 50 µM LBA. (i) Same as (g) but with 50 µM LBA (n = 5). All cellular assays were repeated three times and are displayed as mean + SEM.

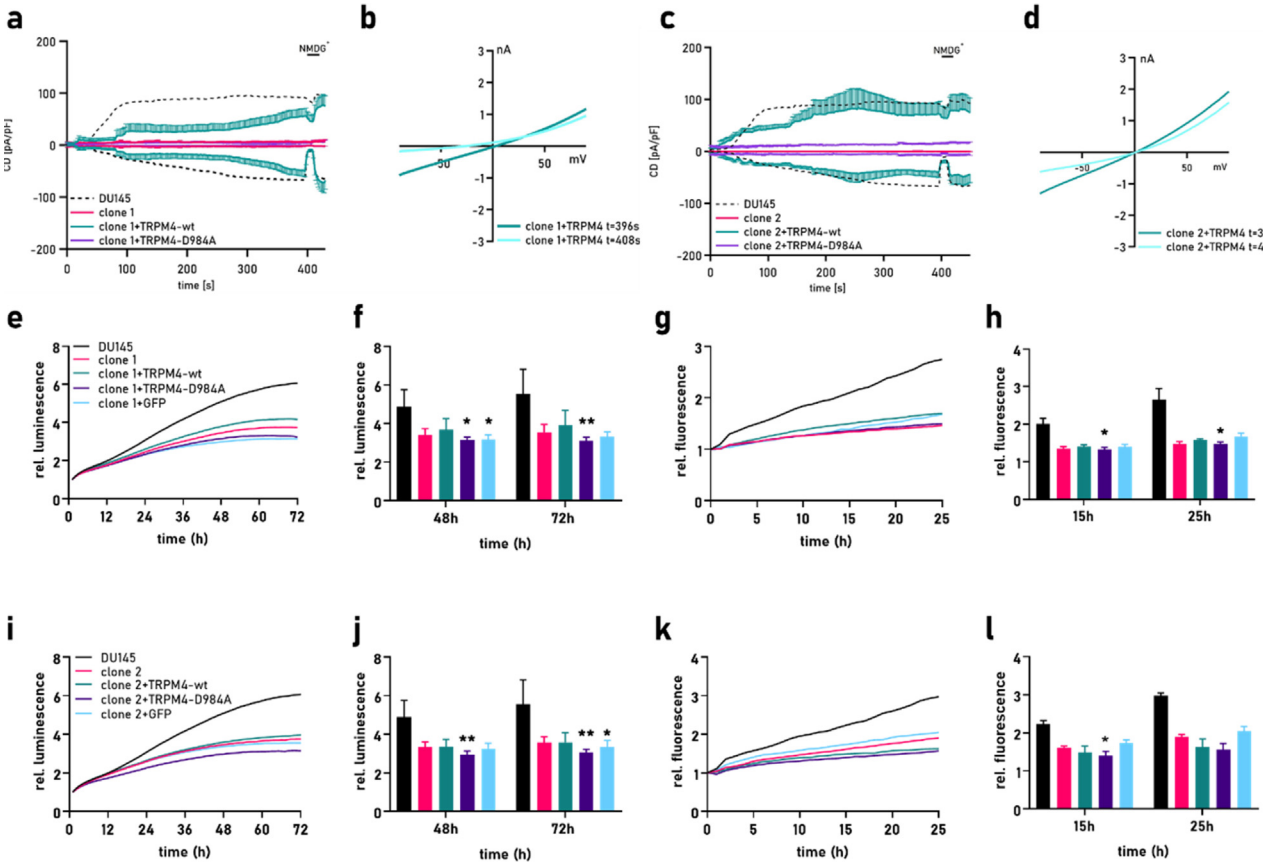

Figure 6. TRPM4 rescue experiment with clones 1 and 2. (a) Whole-cell patch clamp data of clone 1 transfected with TRPM4-wt or TRPM4 dominant negative constructs (TRPM4-D984A), activated with 10 μM Ca^{2+} in patch pipette ($n = 5$ for DU145, $n = 4$ for clone 1, $n = 7$ for clone 1 + TRPM4-wt, $n = 7$ for clone 1 + TRPM4-D984A). $NMDG^+$ was applied on cells at $t = 400$ s. (b) IVs at $t = 396$ s and during application of $NMDG^+$ ($t = 408$ s). (c) Same as (a) for clone 2 ($n = 5$ for DU145, $n = 5$ for clone 2, $n = 5$ for clone 2 + TRPM4-wt, $n = 4$ for clone 2 + TRPM4-D984A). (d) Same as (b) for clone 2. (e) Viability assay of DU145, clone 1, clone 1 + TRPM4-wt, clone 1 + TRPM4-D984A, and clone 1 + GFP measured over 72 h. (f) Bar graph of cell viability at 48 and 72 h for clone 1 rescue cells from experiment in (e). (g) Transwell migration of DU145, clone 1, clone 1 + TRPM4-wt, clone 1 + TRPM4-D984A, and clone 1 + GFP. Relative fluorescence plotted over 25 h. (h) Migration of cells from (g) at 15 and 25 h. (i) Viability assay of DU145, clone 2, clone 2 + TRPM4-wt, clone 2 + TRPM4-D984A, and clone 2 + GFP measured over 72 h. (j) Bar graph of cell viability at 48 and 72 h for clone 2 rescue cells from experiment in (i). (k) Transwell migration of DU145, clone 2, clone 2 + TRPM4-wt, clone 2 + TRPM4-D984A, and clone 2 + GFP. Relative fluorescence plotted over 25 h. (l) Migration of cells from (k) at 15 and 25 h. Assays were repeated three times and are displayed as mean + SEM, and p-value < 0.05 was considered significant.

clamp experiments (Figure 6a–d). TRPM4-specific currents were recovered in both K.O. clones re-expressing TRPM4-wt, but not in cells expressing TRPM4-D984A. Application of $NMDG^+$ to the bath solution (at $t = 400$ s) blocked the inward current, confirming that the Ca^{2+} activated current was carried by TRPM4-dependent Na^+ influx.

Changes in viability were analyzed in TRPM4-K.O. cells with re-expression of the two TRPM4 constructs. Re-expression of functional TRPM4-wt caused partial recovery of viability in clone 1. Expression of TRPM4-D984A, on the other hand, was not able to recover the decrease in viability observed in the TRPM4-K.O. cells (Figure 6e and f). Cell migration could not be rescued with TRPM4 re-expression in clone 1 (Figure 6g and h). Rescue experiments with clone 2 were non-conclusive (Figure 6i-l). Additional assays, such as cell adhesion evaluated with impedance-based assay (data not shown) and the imaged-based cell confluence assay (see Supplementary Figure S4), were inconclusive probably due to changes in cell size and shape in the different knockout and knock-in systems.

Next, cell cycle distribution was analyzed in cells re-expressing TRPM4. Clone 1, with both re-expressing TRPM4-wt and expression of TRPM4-D984A, recovered the lower percentage of cells in G1-phase, as seen in DU145 cells (Figure 7a and b). The control cells expressing empty vector with

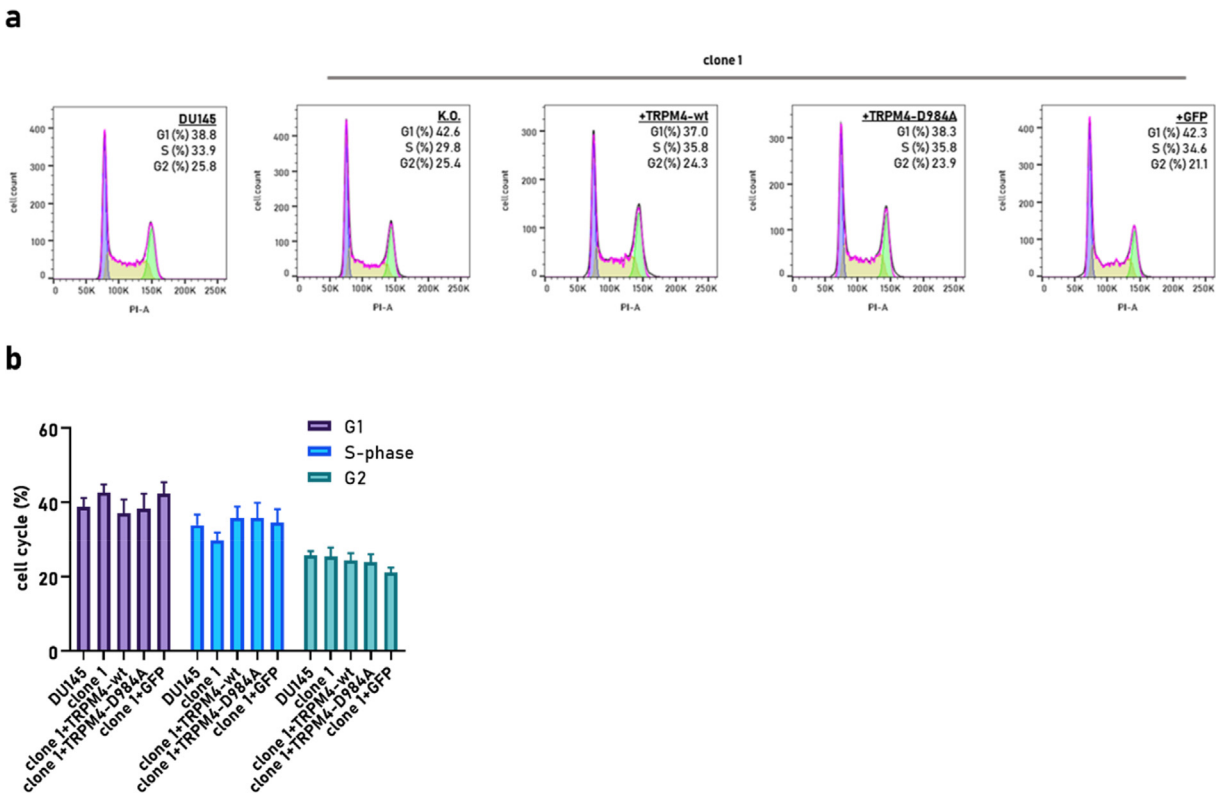

Figure 7. Cell cycle distribution after re-expression of TRPM4. (a) Representative histograms of the cell cycle distribution of DU145, clone 1, clone 1 + TRPM4-wt, clone 1 + TRPM4-D984A, and clone 1 + GFP based on PI staining. (b) Bar graph of cell cycle distribution of clone 1 re-expressing TRPM4-wt or D984A mutant presented as % of cells + SEM from at least three independent experiments.

GFP remained unchanged in comparison to the TRPM4-K.O. cells. For clone 2, no rescue effect was observed with TRPM4-wt or with TRPM4-D984A (Supplementary Figure S5).

In summary, TRPM4-wt could partially rescue the viability phenotype, while TRPM4-D984A failed to rescue the phenotype. In addition, TRPM4 was able to rescue the cell cycle shift in G1-phase observed in TRPM4-K.O. clone 1.

Expression of TRPM4 in prostate cancer tissue

Next, to investigate the association between TRPM4 expression and disease progression, we measured the expression of TRPM4 on a prostate cancer tissue microarray (TMA) assembled by the European Multicenter Prostate Cancer Clinical and Translational Research (EMPaCT) initiative.[31] No association between TRPM4 and overall survival probability was identified (Supplementary Figure S6a, pairwise comparison using log-rank test in Supplementary Table S1). While no association between TRPM4 expression and PSA or disease progression was identified (Supplementary Figure S6b and c, pairwise comparison with log-rank test in Supplementary Tables S2 and S3), we found a positive association between TRPM4 and local/metastatic progression (log-rank pairwise adjusted *p*-value = 0.05, between score 3 v.s. score 4, Supplementary Figure S6d, Supplementary Table S4).

Discussion

Lately, interest in the role of ion channels in cancer development and progression has increased.[32–35] Several TRP channel family members have been reported to be overexpressed in different types of cancer[33] and TRPM8, TRPV6, TRPC6, TRPV2, and TRPA1 have been shown to be involved in prostate cancer progression.[36] In the last years, TRPM4, a member of the TRP channel superfamily, has received increasing interest for its involvement in prostate cancer. TRPM4 has been linked to migration of prostate cancer cell lines.[9,18,21] In this study, we confirm these findings with a stable knockout system in DU145 cells. In addition, reduced proliferation has been reported in PC3 cells upon TRPM4 shRNA downregulation.[17,21] While another study reported no changes in PC3 or DU145 upon siRNA downregulation,[9] we here report a strong decrease in both proliferation and viability of DU145 TRPM4-K.O. cells. Furthermore, TRPM4 has been investigated for its potential as a biomarker for prostate cancer disease progression. In 2015, Holzmann and colleagues

analyzed TRPM4 tissue expression in a small group of 20 prostate cancer patients.[9] They reported elevated TRPM4 expression in prostatic intraepithelial neoplasia (PIN) compared to healthy tissue. However, no correlation between TRPM4 and pathological stages or clinical outcome was observed. One year later, in a bigger cohort study, Berg *et al.* analyzed TRPM4 expression in tissue samples from 614 prostate cancer patients.[4] Here, a significantly higher staining intensity of TRPM4 was reported in cancerous prostates compared to matched benign glands. No direct significant correlation between TRPM4 expression and risk of biochemical recurrence was detected. However, samples with an H-score equal to or above median, in combination with high-intensity TRPM4 staining, significantly correlated with an increased risk of biochemical recurrence. In the current study we report a positive correlation between TRPM4 staining intensity (score 3 vs. score 4) and local/metastatic progression.

As more studies show the potential involvement of TRPM4 in prostate cancer pathophysiology, there is a need for novel tools, such as selective and potent inhibitors, to further study its role. In this study, we evaluated three novel TRPM4 blockers for their potency to block the current of endogenously expressed TRPM4 in prostate cancer cells. The two CBA derivatives, LBA and NBA,[25,26] showed inhibitory effects on the Ca^{2+} activated TRPM4 current. Nevertheless, none of these blockers had any TRPM4 specific effect on prostate cancer cell proliferation or migration, possibly as the blockers did not inhibit the entire current at low micromolar concentrations. In the case of DU145, cells treated with 50 μM NBA or LBA still retained 12–15% of the original current. Moreover, the lack of effect on cell proliferation and migration could indicate that TRPM4-mediated ion conductivity is not needed for the observed effect in knockout and knockdown systems. Potentially the observed effect is due to protein expression rather than the activity of TRPM4. Nonetheless, our data from experiments investigating DU145 TRPM4-K.O. cells re-expressing TRPM4-wt or TRPM4-D984A point to a role for TRPM4 current in cell viability. A recent publication showed that TRPM4-mediated ion conductivity is required for the rescue of viability and cell cycle shift in a colorectal cancer cell line.[27] However, if this is also the case for prostate cancer needs further investigation, including a detailed analysis of SOCE, that is impaired upon downregulation of TRPM4 and plays a pivotal role in cancer cell progression.[37,38] A previous study showed a 50% increased Ca^{2+} entry rate and 20% higher Ca^{2+} plateau in DU145 TRPM4 knockdown cells with only 40% transfection efficiency, indicating that reduced TRPM4 currents may still affect calcium signaling.[9]

Following this study it would be interesting to analyze the differences in effect of blockers in long term vs short term treatments. As we have learned in this study, long term treatment of cells displays a potential toxic effect on cells in the highest concentrations (25–50 μM) which does not seem to be TRPM4-specific. Possibly short term treatment could be less harmful for the cells.

Changes in proliferation are often linked to modifications of cell cycle progression. We observed here a trend for shift in cell cycle distribution of TRPM4-K.O. clone 1 with a higher percentage of cells in G1-phase when compared to DU145 cells. These alterations are in agreement with recently published data on PC3 cells, for which increased G1-phase and decreased S-phase in TRPM4 depleted cells was reported.[21]

Consistent with the recent study by Hong *et al.*, which reports morphological changes of PC3 prostate cancer cells upon TRPM4 inhibition with miR-150 or siRNA silencing,[21] we observed altered morphology in TRPM4-depleted cells. DU145 TRPM4-K.O. cells appeared more elongated and had more filopodia-like structures compared to the more evenly shaped parental cells. TRPM4 was previously shown to localize in FA and to be involved in FA turnover.[19] Cáceres and colleagues reported diminished cell size upon inhibition of TRPM4 in mouse embryonic fibroblasts. In that study, 9-phenanthrol-treated cells displayed diminished lamellipodia-like actin distribution, suggesting involvement in cell spreading and cytoskeleton reorganization. Based on our impedance-based cellular assay and image-based analysis, we here report a decrease in adhesion of cells without TRPM4 expression. To our knowledge, this is the first time that TRPM4 has been shown to be involved in cell adhesion through a quantificational experimental setup.

The increasing evidence for the involvement of TRPM4 in prostate cancer pathophysiology suggests that TRPM4 is an interesting drug candidate for anti-cancer therapy. Our study reports impaired migration, viability, proliferation, cell cycle shift and a decrease in the adhesion of cells, which lack TRPM4. The fact that ion conductivity plays a role in viability further supports the need for the development and application of potent and specific TRPM4 blockers. Other mechanisms for TRPM4 i.e. protein-protein interaction have lately been reported [46,47] and will be investigated in the context of prostate cancer hallmarks the future. Altogether, our results add to the current interest in the involvement of TRPM4 in cancer characteristics, such as survival, migration, and adhesion.

Material and methods

Cell culture

DU145 cells were purchased from the American Type Culture Collection (ATCC) and cultured in

Minimum Essential Medium (MEM; Gibco) supplemented with 10% v/v fetal calf serum (FCS; Gibco), 1% v/v L-glutamine (Gibco), and 1% v/v Non-Essential Amino Acids (NEAA; Gibco). Stable TRPM4 re-expressing cells were cultured under the selective pressure of 0.5 μg/mL Puromycin (Gibco). All cells were passaged every 3–4 days.

Generation of knockout cell lines

TRPM4-knockout cell lines were generated using CRISPR/Cas9 technique. Two gRNAs were designed and approximately 10 kb were deleted between exon 2 and exon 4 (Chr 19: 95975–105719 9744bp). Sense and antisense oligos for the gRNAs[27] were cloned into pSpCas9(BB)-2A-GFP or pU6-(BbsI)-CBh-Cas9-T2A-mCherry according to the protocol from Zhang Lab.[39] Cells were transfected with the 4D-Nucleofactor X-unit (Lonza) according to the manufacturer's instructions. For each transfection of 2×10^6 cells, 2 μg of each gRNA plasmid (gRNA4.1/gRNA4.2) was used. Twenty-four hours post transfection the cells were sorted for GFP/mCherry in the ASTRIOS flow cytometry sorter (Beckman Coulter). Single cells were seeded in 96-well plates for expansion, and approximately two weeks later single cell clones were transferred to 24-well plates. Around 100 clones were screened by genotyping (primer pairs; see.[27] Clones which showed the desired deletion in both alleles were amplified and then stored in liquid N_2. Cell pellets were collected and further validated with Western blot and quantitative RT-PCR.

Stable re-expression of TRPM4-wt and TRPM4-D984A in TRPM4 knockout cells

DU145 TRPM4-K.O. clones 1 and clone 2 were stably transfected with GFP-tagged TRPM4-wt or TRPM4-D984A dominant-negative constructs to generate stably TRPM4 re-expressing cells. Control cells were transfected with a vector expressing only GFP. The two TRPM4 constructs were amplified from TRPM4-pMaxGFP and TRPM4-D984A-pMaxGFP vectors and GFP was amplified from TRPM4-pMaxGFP (primers listed in[27] and cloned into a piggyBac vector (5753 bp) with ClonExpress® Entry One Step Cloning Kit (Lubio Science) according to the manufacturer's instructions. The cells were co-transfected with 0.5 μg transposase vector and 2 μg of corresponding piggyBac vector using FuGENE transfection kit (Promega). Following that, 72 h post transfection, cell culture medium was replaced with selection medium containing 1 μg/mL Puromycin (Gibco). After two days with high selection pressure, transfected cells were maintained in culture under a lower selection pressure of 0.5 μg/mL Puromycin. Successful re-expression of TRPM4 was confirmed by green fluorescence of transfected cells.

Drug treatment

Three TRPM4 inhibitors were evaluated with cellular assays: 4-chloro-2-(2-chlorophenoxy) acetamido)benzoic acid (CBA), 4-chloro-2-(2-(4-chloro-2-methylphenoxy) propanamido) benzoic acid (LBA), and 4-chloro-2-(1-naphthyloxyacetamido)benzoic acid (NBA). For use in the assays, the compounds were dissolved in dimeythylsulfoxide (DMSO). In control samples, 0.1% DMSO was applied. Proliferation and migration were analyzed with the label-free xCELLigence system (described below).

Western blot

Total cell lysate was prepared using M-PER Mammalian Protein Extraction Reagent (Thermo Scientific) plus protease inhibitor (Halt Protease Inhibitor Cocktail) and benzonase nuclease. Protein concentrations were measured with a Pierce™ BCA Protein Assay Kit (Thermo Scientific), and 50 μg of total protein lysate was loaded onto 10% SDS-PAGE gels (TGX polyacrylamide gel, Bio-Rad). After proteins were transferred to nitrocellulose membrane, TRPM4 was detected with a polyclonal rabbit antibody previously described (1:500)[26]. β-actin, used as endogenous control, was detected with mouse β-actin antibody (1:2000; Cell Signaling Technology, #3700). Both proteins were detected in combination with fluorescent secondary antibodies IRDye® Donkey anti-Mouse (#925-68022, LI-COR) and IRDye® 800CW Goat anti-Rabbit (#925-32211, LI-COR). Protein expression was acquired with the LICOR Odyssey Imaging System (LI-COR Biotechnology) and quantified using Image Studio Lite software (LI-COR Biosciences).

Quantitative real-time PCR (qRT-PCR)

RNA was extracted using QIAshredder and the RNeasy Mini kit (Qiagen) according to the manufacturer's instructions. Reverse transcription of 2 μg was performed with the High-Capacity cDNA Reverse Transcription Kit (Thermo Fisher Scientific). The cDNA was diluted 1:4 and evaluated with quantitative expression analysis using TaqMan Gene Expression Assay (Thermo Fisher Scientific) on the ViiA 7 Real-Time PCR System (Applied Biosystems/Thermo Fisher Scientific) with the following program: 2 min activation at 50 °C, 10 min hold at 95 °C, 40 cycles of 15 s denaturation at 95 °C, and 1 min annealing at 60 °C. The qRT-PCR results were analyzed with the $\Delta\Delta C_t$ method and expression levels were normalized to two housekeeping genes: RNA polymerase II (RNAPol II, Hs00172187_m1) and TATA-binding protein (TBP, Hs00427621_m1). TRPM4 mRNA expression was quantified with Hs01026061_m1 primer-probe mix spanning exon 3–4.

Electrophysiology

Whole-cell patch clamp experiments were performed in LNCaP and DU145 cells at 22–25 °C. Voltage ramps of 50 ms, spanning −100 to +100 mV from a holding potential of 0 mV, were delivered every 2 seconds using the HEKA EPC-10 amplifier. Currents were acquired, digitized, recorded, and analyzed with a HEKA EPC-10 amplifier, HEKA Patchmaster v2x53, and Igor Pro 6.37 software (WaveMetrics). Currents at −80 mV and +80 mV, normalized to cell capacitance, were plotted against time. The bath solution contained 140 mM NaCl, 0.5 mM $CaCl_2$, 3 mM $MgCl_2$, and 10 mM HEPES. Osmolality was adjusted to 300 mOsm with glucose and pH was set to 7.2 with NaOH or HCl. In the N-methyl-D-glucamine ($NMDG^+$) bath solution, NaCl was replaced by 140 mM $NMDG^+$. The internal pipette solution contained 140 mM Cs-glutamate, 10 mM EDTA, 10 mM HEPES, and 8 mM NaCl. WEBMAXC STANDARD was used for calculation of free Mg^{2+} (3 mM) and Ca^{2+} (10 μM) in the internal pipette solution.[40] Patch pipettes with a resistance of 2–3 MΩ were used in these experiments.

Viability and proliferation assays

RealTime Glo MT Cell Viability Assay (Promega) was used to study cell viability kinetics. Cells were seeded in white 96-well plates at a density of 2×10^3 cells per well. For this assay, 50 μL of assay reagent mix was added to 50 μL of cells in standard culture medium. Luminescence was assessed every hour over 72 h with a Tecan Spark™ 10 M multimode microplate reader (Tecan), utilizing the heat- and gas-control and humidity chamber. Cells were always passaged the day before experimental set up. Each experimental condition was measured in triplicate and repeated three times. All experiments were normalized to the first measured value.

Cell proliferation was assessed with xCELLigence® E-Plates on the xCELLigence® RTCA DP system (ACEA Biosciences), an assay that records changes in impedance as the cells adhere to the surface of the plate. For the proliferation assay, 1×10^4 cells were seeded per well and impedance was measured every 15 min over 72 h. This assay was also used to study the adhesion of cells during the initial hours. Cells were always passaged the day before the experiment was set up and each experiment was repeated a minimum of three times. Statistical significance for viability and proliferation assays was analyzed with the Friedman test and Dunn's test for multiple comparison.

Transwell migration assays

Prior to the migration assay, cells were incubated with 1 μM CellTracker™ Green CMFDA Dye (Invitrogen) in serum-free medium for 30 min. After replacing the medium with fresh serum-free medium, the top chamber of the 24-well plate containing Fluorblok inserts (Corning) was loaded with 5×10^4 fluorescent cells. The bottom chamber of the 24-well plate was filled with normal culture medium with 10% FCS as attractant. Relative fluorescence was measured in top and bottom readout mode every hour over 25 h with the Tecan Spark™ 10 M multimode microplate reader (Tecan) utilizing the gas control and heat settings. The migratory potential of the cells was calculated as the ratio of cells migrating through the pores of the chamber relative to the number of cells remaining in the top chamber.

The xCELLigence system offers a label-free transwell migration assay. For this assay, 4×10^4 cells were seeded in serum-free media in the top chamber of the xCELLigence ® CIM-Plates (ACEA Biosciences). Standard culture medium with 10% FCS as attractant was used in the bottom chamber. Whenever a compound was tested, the inhibitor was added to the top chamber. Impedance was measured in 15 min intervals for 25 h with the xCELLigence ® RTCA DP device. Statistical significance for the two transwell migration assays was analyzed with the Friedman test and Dunn's test for multiple comparison.

IncuCyte live cell imaging

The IncuCyte S3 system (Essen BioScience) was used to analyze cell confluence, cell adhesion, and the average size of objects (cells). Cells were trypsinized, counted, and diluted to 0.5×10^5, 1×10^5, and 2×10^5 cells per well in a 24-well plate. Acquisition was initiated immediately after seeding. Phase contrast images were acquired every 30 min for 24 h, at 10× magnification. All cells were passaged the day before the experiment begun to be in the same growth phase and confluence. Images were analyzed using IncuCyte S3 Software (Essen BioScience). The experiment was repeated at least three times. The Friedman test and Dunn's test for multiple comparison were used for statistical evaluation.

Cell cycle analysis

Propidium iodide (PI) staining was performed with a Propidium Iodide Flow Cytometry Kit (Abcam) according to the standard protocol. Cells were counted and seeded into 6-well plates at a density of 3×10^5 per well the day before fixation. On the following day, cells were collected and fixed in 66% ice-cold EtOH and stored at 4 °C overnight or until FACS analysis. Cell cycle distribution was analyzed with BD LSR II flow cytometer (BD Bioscience) and FACSDiva Software (BD Bioscience). Collected data were

analyzed with FlowJo v10 (FlowJo). Each experiment was repeated at least three times. Statistical significance was analyzed with one-way ANOVA and the Holm-Sidiak' multiple comparison test.

Immunofluorescence and staining quantification

A prostate cancer tissue microarray (TMA) of 210 patient samples assembled from the European Multicenter Prostate Cancer Clinical and Translational Research (EMPaCT) initiative (Ref PMID: 28753838) was used for immunofluorescence (IF) staining. TMA sections were stained for TRPM4 expression by IF using the Tyramide SuperBoost™ kit (Invitrogen). The TMA sections were incubated at 55 °C 2 h prior to deparaffinization and antigen retrieval in boiling citrate buffer. The following IF staining was performed according to the manufacturer's protocol: In short, endogenous peroxidase activity was quenched by 3% H_2O_2 and sections blocked in blocking buffer (10% goat serum) for 1 hour before overnight incubation with the primary polyclonal rabbit antibody against TRPM4 (generated by Pineda, previously described by.[26] The next day, the sections were incubated with poly-HRP-conjugated goat anti-rabbit IgG antibody and tyramide labelling was performed for 5 min. Nuclear counterstaining with DAPI (Thermo Fisher Scientific) was performed and the slides were scanned by a Pannoramic 250 Flash III slide scanner (3D Histech Ltd). IF staining was scored as negative (0) or positive (1–4) by manually counting TRPM4-positive areas, as follows: 0 = no staining; 1 = staining in one area; 2 = staining in two areas; 3 = staining in three areas; 4 = staining in more than three areas.

Survival analysis

Kaplan-Meier curves to illustrate the progression of the stratified scoring groups in the prostate cancer cases were calculated using the "survfit" function and the global log-rank test using the Survival R package.[41,42] For pairwise comparison, p-value was estimated by the log-rank test and adjusted with the Benjamini–Hochberg (BH) method. For all parameters, if no information on patient outcome was available, information at last follow-up was used. Clinical progression was defined as metastasis or local recurrence. Disease progression was defined by combining any form of recurrence (PSA and clinical progression). Data representation and graphical plots were generated using the ggplot2 R package.[43] Data analysis was done using RStudio version 1.1.463[44] and R version 3.5.3.[45]

Statistical analysis

Cellular assays were statistically evaluated with the Friedman test and Dunn's test for multiple comparison. FACS cell cycle data were analyzed with one-way ANOVA and the Holm–Sidak multiple comparison test. All analyses consisted of at least three independent experiments. All data are displayed as mean +/− SEM unless indicated otherwise. Statistical analysis was performed on GraphPad Prism8. Experiments with a p-value < 0.05 were considered significant. The survival analysis was performed on RStudio version 1.1.463.

Ethics statement

The use of patient tissue samples and the linked patient data in this study were approved by the local Ethics Committee of Canton of Bern, Switzerland (permit number KEK-BE: 128/2015).

Acknowledgements

This work was supported by funding from the National Centre of Competence in Research (NCCR) TransCure funded by Swiss National Science Foundation (SNSF). AB acknowledges funding by SNSF Flexibility Grant (51NF40-160620). We thank Prof. Jean-Louis Reymond and Dr. Clémence Delalande for supplying samples of CBA, NBA and LBA. We thank Prof. Hugues Abriel for providing the TRPM4 antibody. TRPM4-wt and TRPM4-D984A constructs were kindly provided by Prof. Thomas Voets and the piggyBac and the transposase vectors were friendly gifts from Prof. Olivier Pertz.

Declaration of Competing Interest

The authors declare that they have no known competing financial interests or personal relationships that could have appeared to influence the work reported in this paper.

Author Contributions

AB and CP conceived the study; AB, CP and BH are responsible for experimental design; AB, BH, SK, EZ, MK, PS, RB conducted the experiments; AB, EZ, MK, SK, BH, RB analyzed and interpreted the data; CP, MKJ, MS, AB were in charge of administration, technical and material support; AB drafted the manuscript and prepared the figures; CP and AB edited and polished the manuscript. All authors read and approved the final manuscript.

Appendix A. Supplementary material

Supplementary Tables S1-4. Pairwise comparison between groups (score 0, 1, 2, 3, and 4), using log-rank test. P-value is adjusted by Benjamini–Hochberg (BH) method. Supplementary data to this article can be found online at https://doi.org/10.1016/j.jmb.2020.09.024.

Received 2 July 2020;
Accepted 29 September 2020;
Available online xxxx

Keywords:
patch-clamp;
small molecule inhibitors;
adhesion;
proliferation;
migration

1 Employers could choose their customized charging demand to be served by WPC. For example, additional miles could be added to allow additional mileages for other travel activity purposes. Also, the actual charging demand could be adjusted if different vehicle types with various fuel economies are considered.

Abbreviations:
TRPM4, transient receptor melastatin 4 channel; **ADT**, androgen deprivation therapy; **CRPC**, castration-resistant prostate cancer; **FA**, focal adhesion; **EMT**, epithelial mesenchymal transition; **IF**, immunofluorescence; **TMA**, tissue microarray

References

1. Bray, F., Ferlay, J., Soerjomataram, I., Siegel, R.L., Torre, L.A., Jemal, A., (2018). Global cancer statistics 2018: GLOBOCAN estimates of incidence and mortality worldwide for 36 cancers in 185 countries. *CA Cancer J. Clin.*, **68**, 394–424.
2. Harris, W.P., Mostaghel, E.A., Nelson, P.S., Montgomery, B., (2009). Androgen deprivation therapy: progress in understanding mechanisms of resistance and optimizing androgen depletion. *Nat. Clin. Pract. Urol.*, **6**, 76–85.
3. Liu, J., Zheng, Y., Gao, Y., Quan, Z., Qiao, B., Li, L., Li, T., Duan, L., Yang, J., Luo, C., Wu, X., (2020). Inhibitor 9 combined with androgen deprivation therapy or chemotherapy delays the malignant behavior of castration-resistant prostate cancer through K-Ras/PLCε/PKCε signaling pathway. *Front. Oncol.*, **10**
4. Berg, K.D., Soldini, D., Jung, M., Dietrich, D., Stephan, C., Jung, K., Dietel, M., Vainer, B., Kristiansen, G., (2016). TRPM4 protein expression in prostate cancer: a novel tissue biomarker associated with risk of biochemical recurrence following radical prostatectomy. *Virchows Arch.*, **468**, 345–355.
5. Schinke, E.N., Bii, V., Nalla, A., Rae, D.T., Tedrick, L., Meadows, G.G., Trobridge, G.D., (2014). A novel approach to identify driver genes involved in androgen-independent prostate cancer. *Mol. Cancer*, **13**, 120.
6. Su, A.I., Wiltshire, T., Batalov, S., Lapp, H., Ching, K.A., Block, D., Zhang, J., Soden, R., Hayakawa, M., Kreiman, G., Cooke, M.P., Walker, J.R., Hogenesch, J.B., (2004). A gene atlas of the mouse and human protein-encoding transcriptomes. *PNAS*, **101**, 6062–6067.
7. Vennekens, R., Nilius, B., (2007). *In: Transient Receptor Potential (TRP) Channels*,. Springer Berlin Heidelberg, 2007, pp. 269–285. doi:10.1007/978-3-540-34891-7_16.
8. Fleig, A., Penner, R., (2004). The TRPM ion channel subfamily: molecular, biophysical and functional features. *Trends Pharmacol. Sci.*, **25**, 633–639.
9. Holzmann, C., Kappel, S., Kilch, T., Jochum, M.M., Urban, S.K., Jung, V., Stöckle, M., Rother, K., Greiner, M., Peinelt, C., (2015). Transient receptor potential melastatin 4 channel contributes to migration of androgen-insensitive prostate cancer cells. *Oncotarget*, **6**, 41783–41793.
10. Vennekens, R., Olausson, J., Meissner, M., Bloch, W., Mathar, I., Philipp, S.E., Schmitz, F., Weissgerber, P., Nilius, B., Flockerzi, V., Freichel, M., (2007). Increased IgE-dependent mast cell activation and anaphylactic responses in mice lacking the calcium-activated nonselective cation channel TRPM4. *Nat. Immunol.*, **8**, 312–320.
11. Launay, P., Cheng, H., Srivatsan, S., Penner, R., Fleig, A., Kinet, J.P., (2004). TRPM4 regulates calcium oscillations after T cell activation. *Science*, **306**, 1374–1377.
12. Ngoc Tran, T.D., Stovall, K.E., Suantawee, T., Hu, Y., Yao, S., Yang, L.J., Adisakwattana, S., Cheng, H., (2017). Transient receptor potential melastatin 4 channel is required for rat dental pulp stem cell proliferation and survival. *Cell Prolif.*, **50**
13. Cheng, H., Beck, A., Launay, P., Gross, S.A., Stokes, A.J., Kinet, J.P., Fleig, A., Penner, R., (2007). TRPM4 controls insulin secretion in pancreatic β-cells. *Cell Calcium*, **41**, 51–61.
14. Kappel, S., Marques, I.J., Zoni, E., Stok, P., Peinelt, C., Mercader, N., Julio, M.K., Borgström, A., (2017). Store-operated Ca 2 + entry as a prostate cancer biomarker — a riddle with perspectives. *Curr. Mol. Biol. Rep.*, **3**, 208–217.
15. Ashida, S., Nakagawa, H., Katagiri, T., Furihata, M., Iiizumi, M., Anazawa, Y., Tsunoda, T., Takata, R., Kasahara, K., Miki, T., Fujioka, T., Shuin, T., Nakamura, Y., (2004). Molecular features of the transition from prostatic intraepithelial neoplasia (PIN) to prostate cancer: genome-wide gene-expression profiles of prostate cancers and PINs. *Cancer Res.*, **64**, 5963–5972.
16. Armisén, R., Marcelain, K., Simon, F., Tapia, J.C., Toro, J., Quest, A.F.G., Stutzin, A., (2011). TRPM4 enhances cell proliferation through up-regulation of the β-catenin signaling pathway. *J. Cell. Physiol.*, **226**, 103–109.
17. Sagredo, A.I., Sagredo, E.A., Cappelli, C., Báez, P., Andaur, R.E., Blanco, C., Tapia, J.C., Echeverría, C., Cerda, O., Stutzin, A., Simon, F., Marcelain, K., Armisén, R., (2018). TRPM4 regulates Akt/GSK3-β activity and enhances β-catenin signaling and cell proliferation in prostate cancer cells. *Mol. Oncol.*, **12**, 151–165.
18. Sagredo, A.I., Sagredo, E.A., Pola, V., Echeverría, C., Andaur, R., Michea, L., Stutzin, A., Simon, F., Marcelain, K., Armisén, R., (2018). TRPM4 channel is involved in regulating epithelial to mesenchymal transition, migration, and invasion of prostate cancer cell lines. *J. Cell. Physiol.*, **234**, 2037–2050.
19. Cáceres, M., Ortiz, L., Recabarren, T., Romero, A., Colombo, A., Leiva-Salcedo, E., Varela, D., Rivas, J., Silva, I., Morales, D., Campusano, C., Almarza, O., Simon, F., Toledo, H., Park, K.-S., Trimmer, J.S., Cerda, O., (2015). TRPM4 is a novel component of the adhesome

required for focal adhesion disassembly, migration and contractility. *PloS One*, **10** e0130540.

20. Blanco, C., Morales, D., Mogollones, I., Vergara-Jaque, A., Vargas, C., Álvarez, A., Riquelme, D., Leiva-Salcedo, E., González, W., Morales, D., Maureira, D., Aldunate, I., Cáceres, M., Varela, D., Cerda, O., (2019). EB1- and EB2-dependent anterograde trafficking of TRPM4 regulates focal adhesion turnover and cell invasion. *FASEB J.*, **33**, 9434–9452.
21. Hong, X., Yu, J.-J., (2019). MicroRNA-150 suppresses epithelial-mesenchymal transition, invasion, and metastasis in prostate cancer through the TRPM4-mediated β-catenin signaling pathway. *Am. J. Physiol.-Cell Physiol.*, **316**, C463–C480.
22. Burris, S.K., Wang, Q., Bulley, S., Neeb, Z.P., Jaggar, J.H., (2015). 9-Phenanthrol inhibits recombinant and arterial myocyte TMEM16A channels. *Br. J. Pharmacol.*, **172**, 2459–2468.
23. Garland, C.J., Smirnov, S.V., Bagher, P., Lim, C.S., Huang, C.Y., Mitchell, R., Stanley, C., Pinkney, A., Dora, K.A., (2015). TRPM4 inhibitor 9-phenanthrol activates endothelial cell intermediate conductance calcium-activated potassium channels in rat isolated mesenteric artery. *Br. J. Pharmacol.*, **172**, 1114–1123.
24. Gardam, K.E., Geiger, J.E., Hickey, C.M., Hung, A.Y., Magoski, N.S., (2008). Flufenamic acid affects multiple currents and causes intracellular Ca^{2+} release in *Aplysia* bag cell neurons. *J. Neurophysiol.*, **100**, 38–49.
25. Delalande, C., Awale, M., Rubin, M., Probst, D., Ozhathil, L.C., Gertsch, J., Abriel, H., Reymond, J.-L., (2019). Optimizing TRPM4 inhibitors in the MHFP6 chemical space. *Eur. J. Med. Chem.*, **166**, 167–177.
26. Ozhathil, L.C., Delalande, C., Bianchi, B., Nemeth, G., Kappel, S., Thomet, U., Ross-Kaschitza, D., Simonin, C., Rubin, M., Gertsch, J., Lochner, M., Peinelt, C., Reymond, J.-L., Abriel, H., (2018). Identification of potent and selective small molecule inhibitors of the cation channel TRPM4. *Br. J. Pharmacol.*, **175**, 2504–2519.
27. Kappel, S., Stokłosa, P., Hauert, B., Ross-Kaschitza, D., Borgström, A., Baur, R., Galván, J.A., Zlobec, I., Peinelt, C., (2019). TRPM4 is highly expressed in human colorectal tumor buds and contributes to proliferation, cell cycle, and invasion of colorectal cancer cells. *Mol. Oncol.*, **13**, 2393–2405.
28. Cunningham, D., You, Z., (2015). In vitro and in vivo model systems used in prostate cancer research. *J. Biol. Methods*, **2**, 17.
29. Kho, D., MacDonald, C., Johnson, R., Unsworth, C., O'Carroll, S., Mez, E., Angel, C., Graham, E., (2015). Application of xCELLigence RTCA biosensor technology for revealing the profile and window of drug responsiveness in real time. *Biosensors*, **5**, 199–222.
30. Nilius, B., Prenen, J., Janssens, A., Owsianik, G., Wang, C., Zhu, M.X., Voets, T., (2005). The selectivity filter of the cation channel TRPM4. *J. Biol. Chem.*, **280**, 22899–22906.
31. Tosco, L., Laenen, A., Briganti, A., Gontero, P., Karnes, R. J., Bastian, P.J., Chlosta, P., Claessens, F., Chun, F.K., Everaerts, W., Gratzke, C., Albersen, M., Graefen, M., Kneitz, B., Marchioro, G., Salas, R.S., Tombal, B., Van den Broeck, T., Van Der Poel, H., Walz, J., De Meerleer, G., Bossi, A., Haustermans, K., Van Poppel, H., Spahn, M., Joniau, S., (2018). The EMPaCT classifier: A validated tool to predict postoperative prostate cancer-related death using competing-risk analysis. *Eur. Urol. Focus*, **4**, 369–375.
32. Stock, C., Schwab, A., (2015). Ion channels and transporters in metastasis. *Biochim. et Biophys. Acta – Biomembr.*, **1848**, 2638–2646.
33. Shapovalov, G., Ritaine, A., Skryma, R., Prevarskaya, N., (2016). Role of TRP ion channels in cancer and tumorigenesis. *Sem. Immunopathol.*, **38**, 357–369.
34. Lang, F., Stournaras, C., (2014). Ion channels in cancer: Future perspectives and clinical potential. *Philos. Trans. Roy. Soc. B: Biol. Sci.*, **369**
35. Stokłosa, P., Borgström, A., Kappel, S., Peinelt, C., (2020). TRP channels in digestive tract cancers. *Int. J. Mol. Sci.*, **21**
36. Bernardini, M., Brossa, A., Chinigo, G., Grolez, G.P., Trimaglio, G., Allart, L., Hulot, A., Marot, G., Genova, T., Joshi, A., Mattot, V., Fromont, G., Munaron, L., Bussolati, B., Prevarskaya, N., Pla, A.F., Gkika, D., (2019). Transient receptor potential channel expression signatures in tumor-derived endothelial cells: Functional roles in prostate cancer angiogenesis. *Cancers*, **11**
37. Parekh, A.B., (2010). Store-operated CRAC channels: Function in health and disease. *Nat. Rev. Drug Discovery*, **9**, 399–410.
38. Chen, Y.F., Lin, P.C., Yeh, Y.M., Chen, L.H., Shen, M.R., (2019). Store-Operated Ca2+ entry in tumor progression: From molecular mechanisms to clinical implications. *Cancers*, **11**
39. ZhangLab, 2019, CRISPR Genome Engineering Toolbox at <https://media.addgene.org/cms/filer_public/e6/5a/e65a9ef8-c8ac-4f88-98da-3b7d7960394c/zhang-lab-general-cloning-protocol.pdf>
40. WEBMAXC STANDARD, 2019, at <https://somapp.ucdmc.ucdavis.edu/pharmacology/bers/maxchelator/webmaxc/webmaxcS.htm>
41. T.M. Therneau, A Package for Survival Analysis in S, 2015.
42. Therneau, T.M., Grambsch, P.M., (2000). Modeling Survival Data : Extending the Cox Model. Springer. 2000.
43. Wickham, H., (2016). ggplot2: elegant graphics for data analysis. Springer, New York. 2016, doi:10.1007/978-0-387-98141-3.
44. R Studio Team: RStudio Integrated Development for R. RStudio, 2016.
45. R Core Team: R: A Language and Environment for Statistical Computing, 2019.
46. Rivas José, et al., (2020). KCTD5, a novel TRPM4-regulatory protein required for cell migration as a new predictor for breast cancer prognosis. *The FASEB Journal*,. https://doi.org/10.1096/fj.201901195RRR.
47. Yan Jing, et al., (2020). Coupling of NMDA receptors and TRPM4 guides discovery of unconventional neuroprotectants. *Science*. https://doi.org/10.1126/science.aay3302.